Electronic Supplementary Material (ESI) for Journal of Materials Chemistry C.


# Carbon-Quantum-Dot-Hybridized $NiO_x$ Hole-Transport Layer Enables Efficient and Stable Planar p-i-n Perovskite Solar Cells with High Open-Circuit Voltage

Xuefeng Xia[1], Dan Zhang[1], Xiaofeng Wang[1], Zonghu Xiao[2], Fan Li*[1]

[1]Department of Materials Science and Engineering, Nanchang University, 999 Xuefu Avenue, Nanchang 330031, China

[2]Jiangxi Key Laboratory of Advanced Materials and Applications for Solar Cells, Xinyu University, Xinyu 338004, China

**Author Information**

**Corresponding Author**

Fan Li, E-mail: lfan@ncu.edu.cn

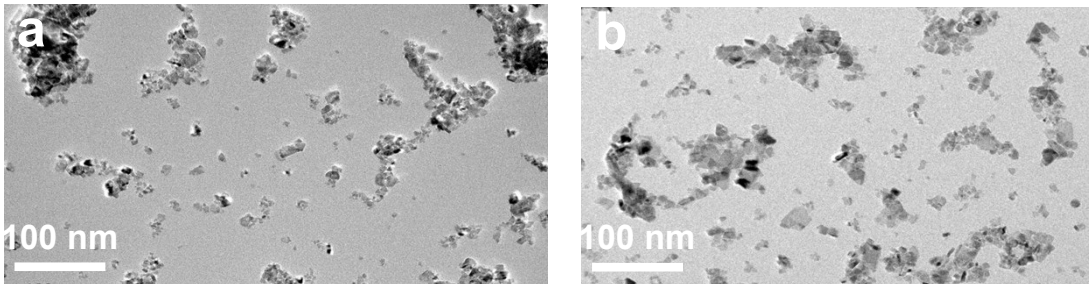


**Figure S1**. TEM images of a) the pristine $NiO_x$ and b) CQDs-hybridized $NiO_x$ dispersed in deionized water.

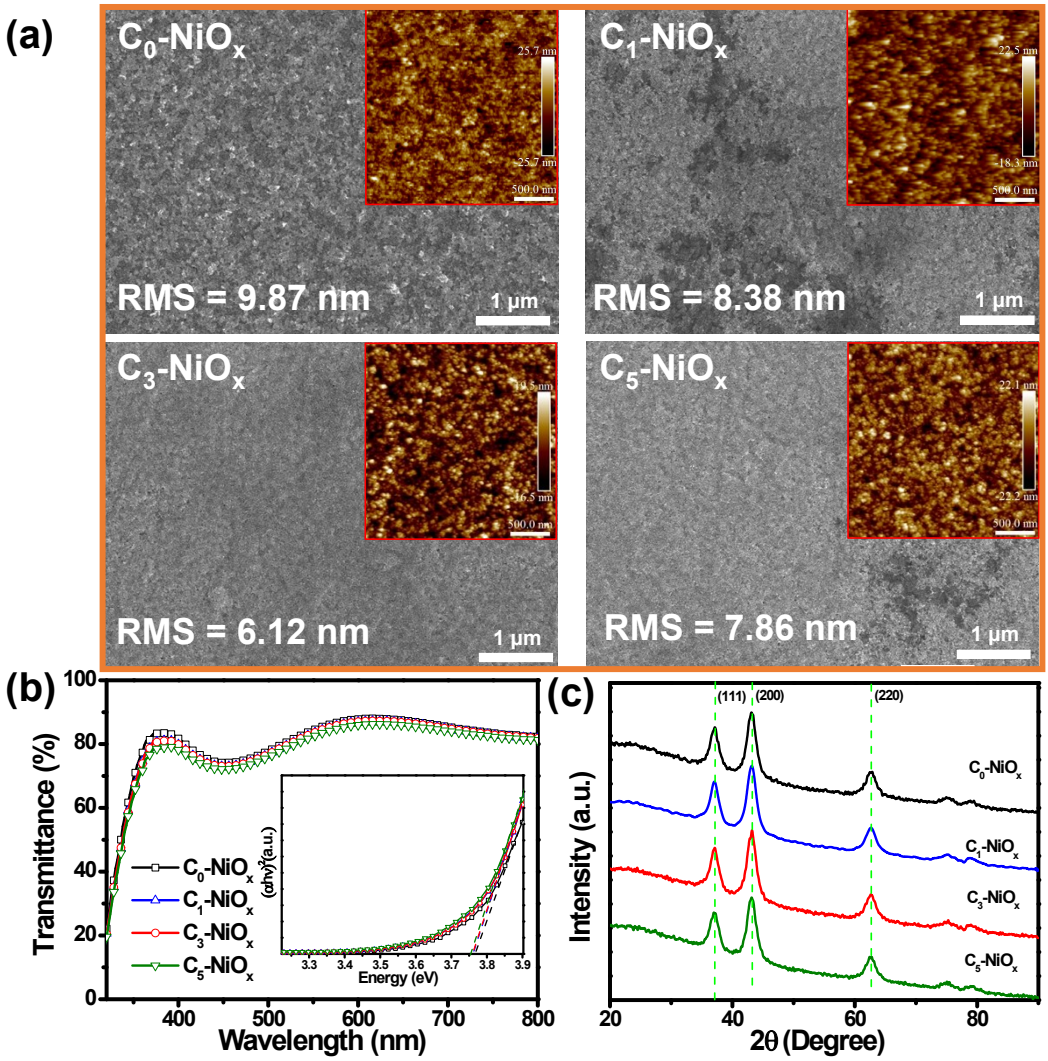


**Figure S2**. (a) FE-SEM and AFM (inset) images, (b) Optical transmittance (Inset: the corresponding Tauc plot of each film) and (c) X-ray diffraction spectra of the $C_0$-$NiO_x$, $C_1$- $NiO_x$, $C_3$- $NiO_x$ and $C_5$- $NiO_x$ films prepared on quartz substrates.

**Table S1. Performance of the reported inverted planar $MAPbI_3$ PSCs based on $NiO_x$ HTLs**

| Device configuration | $V_{oc}$ (V) | $J_{sc}$ (mA $cm^{-2}$) | *FF* | PCE | Method | HTL | Ref |
|---|---|---|---|---|---|---|---|
| ITO/Cu:$NiO_x$/$MAPbI_3$/$PC_{61}BM$/bis-$C_{60}$/Ag | 1.11 | 19.01 | 0.73 | 15.40 | sol-gel | Cu:$NiO_x$ | [1] |
| ITO/Cu:$NiO_x$/ $MAPbI_3$/$C_{60}$/bis-$C_{60}$/Ag | 1.05 | 20.53 | 0.72 | 15.52 | combustion | Cu: $NiO_x$ | [2] |
| ITO/Cu:$NiO_x$/$MAPbI_3$/$C_{60}$/BCP/Ag | 1.12 | 22.28 | 0.81 | 20.26 | NP ink | Cu: $NiO_x$ | [3] |
| ITO/Cu:$NiO_x$/Cysteine/$MAPbI_3$/PCBM/Bphen/Al | 1.11 | 23.60 | 0.70 | 18.30 | combustion | Cu: $NiO_x$ | [4] |
| FTO/Cu:$NiO_x$/$MAPbI_3$/PCBM /Ag | 1.06 | 20.79 | 0.67 | 14.88 | DCMS | Cu: $NiO_x$ | [5] |
| ITO/Ag:$NiO_x$/$MAPbI_3$/$PC_{71}BM$/BCP /Ag | 1.08 | 19.70 | 0.80 | 16.86 | sol-gel | Ag: $NiO_x$ | [6] |
| ITO/Co:$NiO_x$/$MAPbI_3$/PCBM/PEI/Ag | 1.05 | 22.30 | 0.79 | 18.60 | combustion | Co: $NiO_x$ | [7] |
| FTO/Zn:$NiO_x$/$MAPbI_3$/PCBM/BCP/Ag | 1.10 | 22.80 | 0.78 | 19.6 | sol-gel | Zn: $NiO_x$ | [8] |
| FTO/LiNiO/$MAPbI_{3-x}Cl_x$/PCBM/Ag | 1.12 | 21.79 | 0.74 | 18.00 | magnetron | Li: $NiO_x$ | [9] |
| FTO/$NiMgO_x$/$MAPbI_3$/PCBM/ZnMgO/Al | 1.08 | 21.30 | 0.80 | 18.50 | sol-gel | NiMgO | [10] |
| FTO/ Sr:$NiO_x$ /$MAPbI_3$/PCBM/AgAl | 1.11 | 22.73 | 0.79 | 20.05 | sol-gel | Sr:$NiO_x$ | [11] |
| TO/Cs:$NiO_x$ /$MAPbI_3$/PCBM/ZrAcac/Ag | 1.12 | 21.77 | 0.79 | 19.35 | sol-gel | Cs: $NiO_x$ | [12] |
| ITO/Li, Ag:$NiO_x$/$MAPbI_3$/PCBM/BCP/Ag | 1.13 | 21.29 | 0.80 | 19.24 | sol-gel | Li,Ag: $NiO_x$ | [13] |
| FTO/La:$NiO_x$/$MAPbI_3$/PCBM/BCP/Ag | 1.01 | 21.02 | 0.73 | 15.46 | NP ink | La: $NiO_x$ | [14] |
| ITO/Fe:$NiO_x$/$MAPbI_3$/PCBM/BCP/Ag | 1.08 | 19.10 | 0.84 | 17.40 | spray coating | Fe: $NiO_x$ | [15] |
| FTO/$NiO_x$/$MAPbI_3$/PCBM/Ag | 1.03 | 17.42 | 0.71 | 12.70 | sol-gel | $NiO_x$ | [16] |
| ITO/$NiO_x$ (F4-TCNQ)/$MAPbI_3$/PCBM/BCP/Ag | 1.02 | 20.70 | 0.74 | 15.70 | sol-gel | F4-TCNQ:$NiO_x$ | [17] |
| FTO/S:$NiO_x$ /$MAPbI_3$/PCBM/PPDIN6/Ag | 1.10 | 23.28 | 0.80 | 20.43 | spray coating | S: $NiO_x$ | [18] |
| FTO/$NiO_x$ /$MAPbI_3$/PCBM/Ag | 1.01 | 18.30 | 0.81 | 14.95 | EBPVD | $NiO_x$ | [19] |
| FTO $NiO_x$ /$MAPbI_3$/$C_{60}$/$SnO_2$ NCs/Ag | 1.12 | 21.8 | 0.77 | 18.80 | sol-gel | $NiO_x$ | [20] |
| ITO/NiO/$MAPbI_3$/PCBM/PDINO/Ag | 1.11 | 20.57 | 0.76 | 17.50 | NP ink | $NiO_x$ | [21] |

**Reference:**

[1] J.H. Kim, P.W. Liang, S.T. Williams, N. Cho, C.C. Chueh, M.S. Glaz, D.S. Ginger, A.K. Jen, Adv. Mater. 27 (2015) 695-701.

[2] J.W. Jung, C.C. Chueh, A.K. Jen, A Low-Temperature, Solution-Processable, Adv. Mater. 27 (2015) 7874-7880.

[3] W. Chen, Y. Wu, J. Fan, A.B. Djurišić, F. Liu, H.W. Tam, A. Ng, C. Surya, W.K. Chan, D. Wang, Adv. Energy Mater. 8 (2018) 1703519.

[4] J. He, Y. Xiang, F. Zhang, J. Lian, R. Hu, P. Zeng, J. Song, J. Qu, Nano Energy 45 (2018) 471-479.

[5] A. Huang, L. Lei, Y. Chen, Y. Yu, Y. Zhou, Y. Liu, S. Yang, S. Bao, R. Li, P. Jin, Sol. Energy Mater. Sol. Cells. 182 (2018) 128-135.

[6] Y. Wei, K. Yao, X. Wang, Y. Jiang, X. Liu, N. Zhou, F. Li, Appl. Surf. Sci. 427 (2018) 782-790.

[7] Y. Xie, K. Lu, J. Duan, Y. Jiang, L. Hu, T. Liu, Y. Zhou, B. Hu, ACS Appl. Mater. Interfaces 10 (2018) 14153-14159.

[8] X. Wan, Y. Jiang, Z. Qiu, H. Zhang, X. Zhu, S. Iqbal, X. Liu, C. Xin, B. Cao, ACS Appl. Energy Mater. (2018) acsaem.8b00671-.

[9] W. Nie, H. Tsai, J.-C. Blancon, F. Liu, C.C. Stoumpos, B. Traore, M. Kepenekian, O. Durand, C. Katan, S. Tretiak, Adv. Mater. 30 (2018) 1703879.

[10] G. Li, Y. Jiang, S. Deng, A. Tam, P. Xu, M. Wong, H.S. Kwok, Adv. Sci. (2017) 1700463.

[11] J. Zhang, W. Mao, X. Hou, J. Duan, J. Zhou, S. Huang, W. Ou-Yang, X. Zhang, Z. Sun, X. Chen, Sol. Energy 174 (2018) 1133-1141.

[12] W. Chen, F.Z. Liu, X.Y. Feng, A.B. Djurišić, W.K. Chan, Z.B. He, Adv. Energy Mater. 7 (2017) 1700722.

[13] X. Xia, Y. Jiang, Q. Wan, X. Wang, L. Wang, F. Li, ACS Appl. Mater. Interfaces 10 (2018) 44501-44510.

[14] S. Teo, Z. Guo, Z. Xu, C. Zhang, Y. Kamata, S. Hayase, T. Ma, ChemSusChem 12 (2019) 518-526.

[15] P. Chandrasekhar, Y.-H. Seo, Y.-J. Noh, S.-I. Na, Appl. Surf. Sci. 481 (2019) 588-596.

[16] Y. Qin, J. Song, Q. Qiu, Y. Liu, Y. Zhao, L. Zhu, Y. Qiang, J. Alloys Compounds 810 (2019) 151970.

[17] S. Zhao, J. Zhuang, X. Liu, H. Zhang, R. Zheng, X. Peng, X. Gong, H. Guo, H. Wang, H. Li, Mater. Sci. Semicon. Proc. 121 (2021) 105458.

[18] C. Hu, Y. Bai, S. Xiao, K. Tao, W.K. Ng, K.S. Wong, S.H. Cheung, S.K. So, Q. Chen, S. Yang, Solar RRL 4 (2020) 2000270.

[19] M.I. Hossain, A.K.M. Hasan, W. Qarony, M. Shahiduzzaman, M.A. Islam, Y. Ishikawa, Y. Uraoka, N. Amin, D. Knipp, M. Akhtaruzzaman, Y.H. Tsang, Small Methods 4 (2020) 2000454.

[20] Z. Zhu, Y. Bai, X. Liu, C.C. Chueh, S. Yang, A.K.Y. Jen, Adv. Mater. 28 (2016) 6478-6484.

[21] Y. Hou, W. Chen, D. Baran, T. Stubhan, N.A. Luechinger, B. Hartmeier, M. Richter, J. Min, S. Chen, C.O.R. Quiroz, Adv. Mater. 28 (2016) 5112-5120.

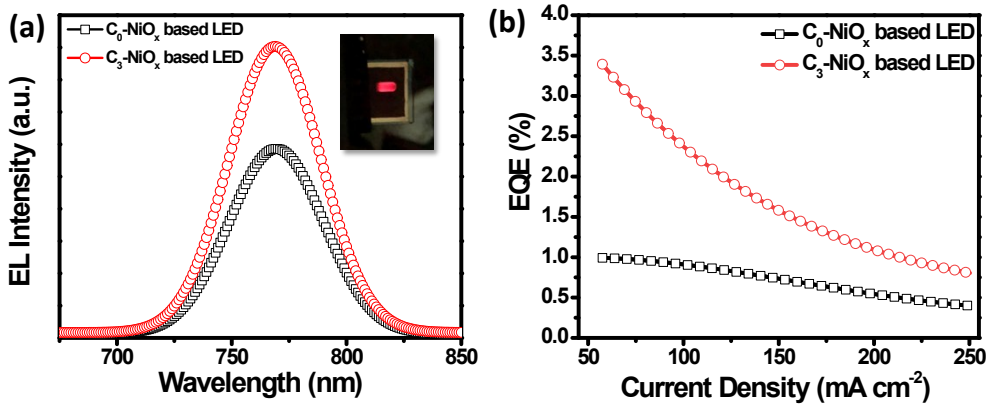


**Figure S3**. a) The electroluminescence spectra (EL) and b) EQE-current density curves for the best-performing $C_0$-$NiO_x$ and $C_3$-$NiO_x$ devics operating as LEDs (Insert: EL image of the $C_3$-$NiO_x$ device).

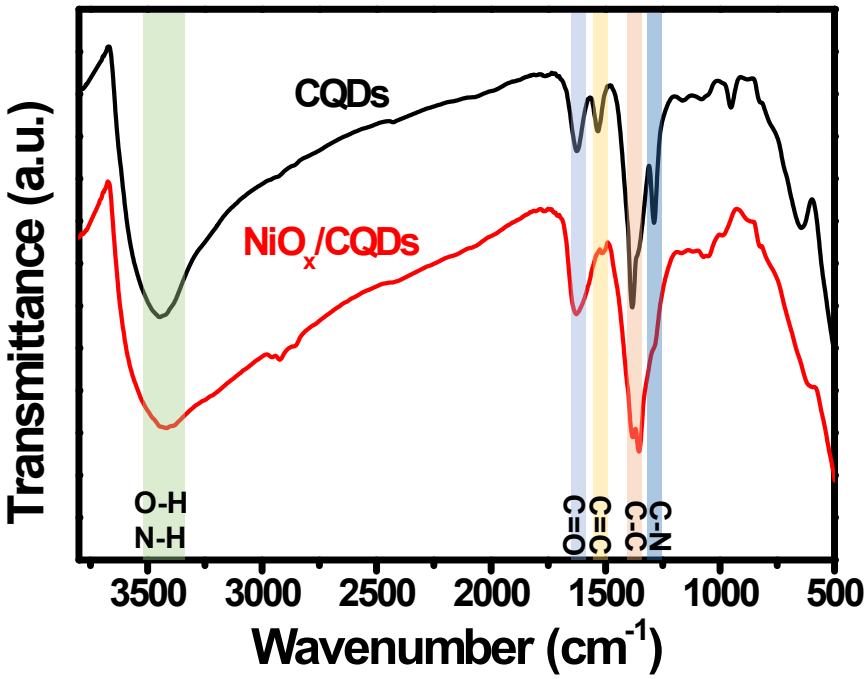


**Figure S4**. FT-IR spectra of the CQDs and CQDs-hybridized $NiO_x$ films.

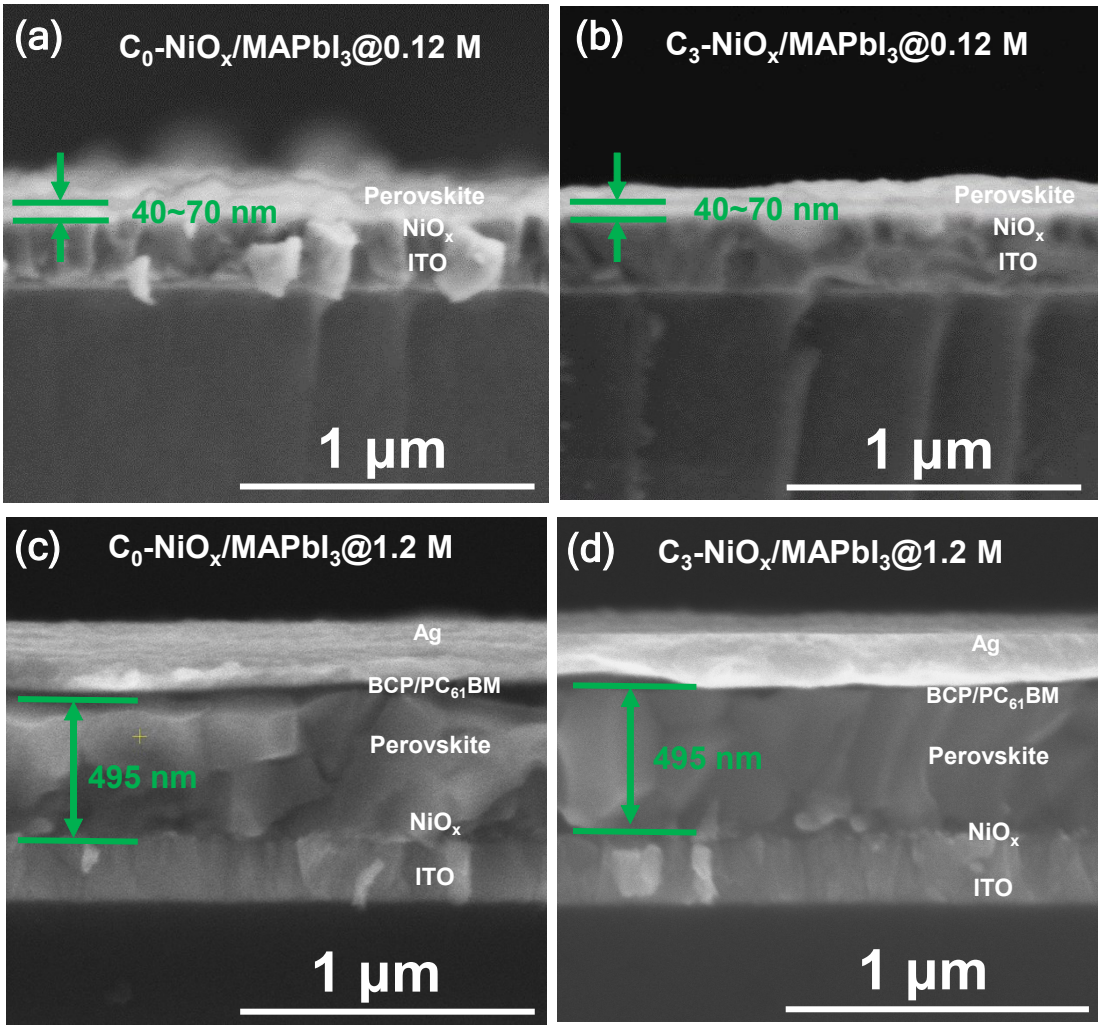


**Figure S5**. The cross-sectional SEM images of (a, b) thin perovskite films (casting from 0.12 M perovskite precursor solution) on $C_0$-$NiO_x$ and $C_3$-$NiO_x$ films, respectively, and (c, d) thick perovskite films (casting from 1.2 M perovskite precursor solution) on $C_0$-$NiO_x$ and $C_3$-$NiO_x$ films, respectively.

**Table S2.** XRD parameters of thin and thick perovskite films on $C_0$-$NiO_x$ and $C_3$-$NiO_x$ HTLs

| Concentrations | Samples | FWHM of (110) (degree) | Intensity ratio of (110) to (310) |
|---|---|---|---|
| 0.12 M | $C_0$-$NiO_x$ | 0.38 | 1.73 |
| | $C_3$-$NiO_x$ | 0.27 | 8.31 |
| 1.20 M | $C_0$-$NiO_x$ | 0.17 | 3.78 |
| | $C_3$-$NiO_x$ | 0.12 | 4.76 |

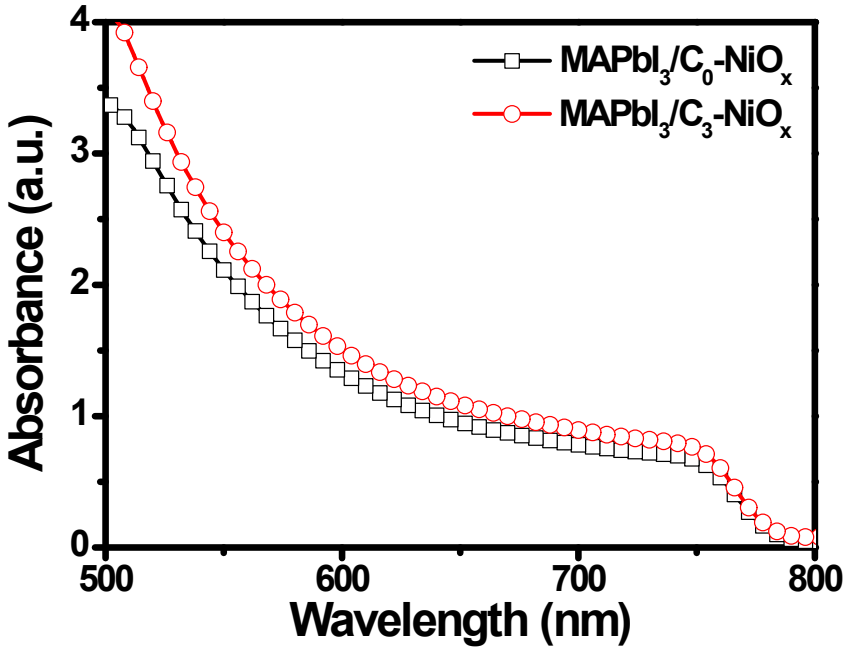


**Figure S6**. UV-vis absorption spectra of thick $MAPbI_3$ films deposited on the $C_0$-$NiO_x$ and $C_3$- $NiO_x$ films.

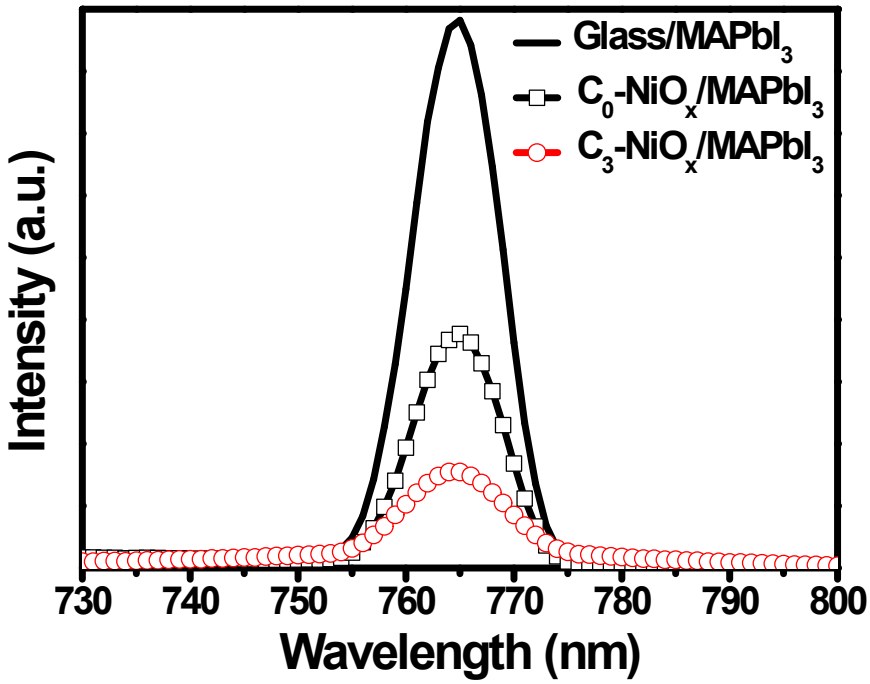


**Figure S7**. Steady-state PL spectra of $MAPbI_3$ perovskite films deposited on the glass, $C_0$-$NiO_x$ and $C_3$-$NiO_x$ films.